



Electrodeposition-assisted formation of anodized TiO₂–CuO heterojunctions for solar water splitting

Saadia Jabeen^{1,6} · Tauqir A. Sherazi¹ · Rahim Ullah² · Syed Ali Raza Naqvi³ · Muhammad Asim Rasheed⁴ · Ghafar Ali⁵ · Atta Ullah Shah² · Yaqoob Khan⁶

Received: 4 July 2020 / Accepted: 8 September 2020 / Published online: 22 September 2020
© King Abdulaziz City for Science and Technology 2020

Abstract

The anatase phase titanium dioxide nanotubes (ATNTs) are investigated for photocatalytic water splitting with and without the formation of copper oxide (CuO) heterojunctions. ATNTs have been grown on titanium substrate by one- and two-step anodization, followed by annealing at 450 °C for transformation to anatase phase. Anodization was performed in an electrolyte containing ammonium fluoride, ethylene glycol and deionized water. The ATNTs were then modified with CuO nanoparticles by dip-coating and electrochemical deposition. The growth of ATNTs and incorporation of CuO nanoparticles in it were confirmed with X-ray diffraction (XRD), field emission scanning electron microscopy (FE-SEM) and energy-dispersive X-ray (EDX) spectroscopy. Well-organized and vertically aligned nanotubes were observed in the FESEM results. Contact angle measurements proved that the thin film of nanotubes is hydrophilic in nature. Linear sweep voltammetry (LSV) technique was performed for photocurrent responses, using distilled water in the dark environment as well as in the light of solar simulator at applied potential of 1.0 V. The photocurrent densities in the dark were negligible, while it became significant under the influence of simulated visible light. The ATNTs grown with two-step anodization offered promising results for photocatalytic water splitting compared to single-step anodization. The CuO modification in ATNTs exhibited a reasonable increase in photocurrent densities compared to pristine ATNTs. Furthermore, the electrochemical deposition process for modification of ATNTs with CuO afforded much better photocurrent responses compared to the dip coating method. The electrochemical deposition of CuO in ATNTs was performed at 0.7 V, 0.9 V and 1.1 V, among which the sample prepared at 0.7 V exhibited the highest photocurrent densities.

Keywords Anodized titania nanotubes (ATNTs) · Heterojunctions · Photoelectrochemical cell (PEC) · Water splitting · Applied bias to photocurrent efficiency (ABPE) · Hydrogen production

✉ Tauqir A. Sherazi
sherazi@cuiatd.edu.pk

✉ Yaqoob Khan
yaqoob@ncp.edu.pk

Saadia Jabeen
saadiamalik09@gmail.com

Rahim Ullah
rahimullahphysics28@gmail.com

Syed Ali Raza Naqvi
draliraza@gcuf.edu.pk

Muhammad Asim Rasheed
masimr22@gmail.com

Ghafar Ali
ghafarali@gmail.com

Atta Ullah Shah
attashah168@gmail.com

¹ Department of Chemistry, COMSATS University Islamabad, Abbottabad Campus, Abbottabad 22060, Pakistan

² National Institute of Lasers and Optronics College, Pakistan Institute of Engineering and Applied Sciences, Islamabad 45650, Pakistan

³ Department of Chemistry, Government College University, Faisalabad 38000, Pakistan

⁴ Department of Physics and Applied Mathematics, Pakistan Institute of Engineering and Applied Sciences, Islamabad 45650, Pakistan

⁵ Nanomaterials Research Group, Physics Division, PINSTECH, Islamabad 45650, Pakistan

⁶ Nanosciences and Technology Department, National Centre for Physics, Quaid-e-Azam University Campus, Islamabad 45320, Pakistan

Introduction

Worldwide energy demand keeps growing and the existing fossil fuels diminish day by day. Coal, oil and natural gas, which are the major energy resources, are in downturn at a rapid rate. The world needs a source of energy which is renewable and sustainable to replenish the need of energy for today and for future. Also, the energy should also be green to fulfill the need of hygienic life. The emission of by-products of carbon due to combustion of fossil fuels degrades the air quality, resulting in climate change worldwide. Hydrogen may be considered as a potential and promising alternative to fossil fuels because of its highest energy production of 120 MJ/kg (Ni et al. 2006). It can be used in fuel cell in the presence of oxygen for electricity generation with the production of harmless water vapor as a by-product. However, the process of production has not progressed yet. The production of hydrogen from water splitting is a most promising alternative to fossil fuel: water is split into H_2 and O_2 molecules in the presence of suitable photocatalyst under sunlight. This solar photocatalytic water splitting is a clean process and has no harmful effects on the environment. However, hydrogen production by this method is not well developed yet. For commercial production of hydrogen, 10% yield has been targeted by researchers using an efficient photocatalyst in the presence of sunlight (Kudo and Miseki 2009). The best photocatalyst must have a narrow bandgap, low electron–hole pair recombination rate, be chemically stable and resistant to corrosion (Praveen Kumar et al. 2013). There are many photocatalysts which are reported with high photocatalytic efficiencies for water splitting including $CaTiO_3$, $MgTiO_3$ – $SrTiO_3$ (Puangpetch et al. 2010), $Au/KTiNbO_5$ (Lin and Chang 2010), $KTa(Zr)O_3$ (Hagiwara et al. 2012), TiO_2 – ZnO (Xie et al. 2017), TiO_2 – ZrO_2 (J. Zhang et al. 2017), etc. But all of these photocatalysts have some limitations in some of the above-mentioned properties. The major problem with these photocatalyst is their activity in UV irradiation with negligible absorption for visible light.

Among the reported photocatalysts, TiO_2 is ideally used practically due to its properties such as suitable band gap, stability in water, non-toxicity, being economical and easy availability (Ge et al. 2016; Hashimoto et al. 2005). Furthermore, TiO_2 in its bulk and thin film form has low photocatalytic efficiency due to limited surface area and larger band gap (> 3 eV). TiO_2 nanotubes synthesized by electrochemical anodization of titanium foil provide parallel electrical channel and large surface area and have proved to be a predominant photocatalyst (Liu et al., 2009). There are three naturally occurring phases of TiO_2 : brookite, anatase and rutile. Among them, the anatase phase is promising

for photocatalytic application due to its high charge carrier mobility (Wold 1993). However, anatase TiO_2 has a wide band gap (3.2 eV) which requires a light source with wavelength less than 387.45 nm to excite an electron from the valence band to the conduction band for causing photocatalytic reaction. TiO_2 may work actively only during UV photons' exposure which shares only 4–5% part of sunlight. Therefore, TiO_2 in the pure form is not effective to be used for photocatalytic water splitting. Some suitable modification is necessary to further enhance its photocatalytic properties. Few successful attempts have been reported by doping various transition metal oxides, i.e., WO_3 (Paramasivam et al. 2010), NiO (Rasheed et al. 2019), rGO (Seong et al. 2018), CuO (Razali and Yusoff 2018) etc.

Among all of these metal oxide semiconductors, CuO is promising for use as a cocatalyst due to its better photochemical properties. CuO has a narrow band gap (1.7 eV) and visible light-active p-type semiconductor. Addition of CuO to TiO_2 nanomaterials improves its photoactivity by means of band gap reduction and charge carrier separation with the help of the CuO/TiO_2 p–n junction (Nguyen et al. 2013).

In this work, the addition of CuO nanoparticles in anodized anatase TiO_2 nanotubes ($CuO/ATNTs$) arrays was studied and its effect on photocatalytic water splitting efficiency presented. A comparative analysis was performed for one- and two-step anodized $CuO/ATNTs$. Two different methods (dip coating and electrodeposition) were followed for CuO addition in $ATNTs$ and their effect on photocatalytic efficiency was studied. The water splitting studies were performed in distilled water, which has not been reported for CuO – $ATNTs$ photocatalyst.

Experimental section

Synthesis of $ATNTs$ by anodization

Titanium (Ti) foil (Good fellow England) having dimensions (1.5 cm length, 1 cm width and 0.02 cm thickness) is used to develop TiO_2 nanotubes. The Ti foil was first washed with deionized water and then degreased by diluted HCl (Sigma-Aldrich), followed by rinsing with deionized water and then ultrasonication for 15 min by 7 ml analytical-grade ethanol (BDH) and 3 ml deionized water. The foils were again washed with deionized water and dried with an air blower. TiO_2 nanotubes were obtained by one- as well as two-step electrochemical anodization processes. In one-step anodization process, 70 mg ammonium fluoride (Sigma-Aldrich, 98+ %), 36 ml ethylene glycol (Sigma-Aldrich, 98+ %) and 1 ml deionized (DI) water were used as the electrolyte in a two-electrode system. The Ti foil acted as an anode or working electrode and graphite rod as a counter electrode.

A DC power supply was used to supply 40 V for 3 h at room temperature between the aforementioned electrodes. The resulting nanotubes were then rinsed with DI water. For the samples to be subjected to two-step anodization, nanotubes obtained from first-step anodization were removed by ultrasonication, followed by the second-step anodization, in which nanotubes were treated for 1 h in fresh electrolyte with the same composition as that used in the first step. After anodization, samples were annealed at 450 °C for 2 h to get the anatase phase of TiO₂. The furnace was ramped at 8 °C per minute for the heating up process and set as 2 °C drop per minute for cooling.

Modification of ATNTs by CuO

The dip coating process was adopted to deposit copper oxide on titania nanotubes. For this purpose, 0.1 molar copper acetate solution (Sigma-Aldrich) and 0.1 molar NaOH (Sigma-Aldrich) solutions were prepared in DI water. The prepared anatase nanotubes were then soaked in copper acetate solution for 1 min, followed by rinsing with DI water and then soaked similarly in NaOH solutions for 1 min, followed by DI water rinsing. The process was repeated ten times. After dip coating, the sample was annealed at 400 °C for 2 h to convert the copper hydroxide into CuO. For electrodeposition of CuO, 0.1 molar copper acetate solution was prepared in DI water and electrodeposited on titania nanotubes using a two-electrode system (titania nanotube film as working electrode and graphite rod as counter electrode) with Gamry potentiostat for 100 s at 0.7 V, 0.9 V and 1.1 V.

Characterization

X-ray diffraction was done for the structural analysis using BRUKER D8 X-ray diffractometer with monochromatic Cu K α 1 radiation ($\lambda = 1.541 \text{ \AA}$, accelerating voltage 40 kV, current of 40 mA). Scanning rate for TiNTs samples was in the 2θ range of 10.0°–70.0° with step size of 0.02° and scanning rate of 1°/min. Analysis of data was done through X'pert High Score software. Field emission scanning electron microscopy was performed by TESCAN FESEM, MAIA3. The scanning was performed in secondary electron imaging mode. EDX spectrometers were installed in the SEM for elemental composition determination. Contact measurement was performed by a goniometer (SEO—Phoenix 150/300 Manual Contact Angle Analyzer).

For water splitting studies, current density vs. voltage curves were obtained using Gamry Instruments potentiostat/galvanostat/ZRA reference 3000. A three-electrode setup was used, in which TiO₂ and CuO/TiO₂ nanotube film was used as the working electrode, platinum wire gauze as the counter electrode and Ag/AgCl as the reference electrode. All of these electrodes were immersed in distilled water

having volume 80 ml. A solar simulator (Keithlink, China) equipped with xenon (Xe) lamp having luminous intensity of 1000 W/m² was used for photocurrent measurements. Light and dark current measurements were done by linear sweep voltammetry (LSV) at the potential range of 0–1 V and scan rate of 10 mV/s at 1 V.

Results and discussion

Structure and morphology analysis

X-ray diffraction (XRD)

Figure 1a, b illustrates the XRD pattern of as-prepared single-step amorphous and 450 °C calcined TNTs. The peaks well matched with JCPDS Card No. 01-084-1286 and 01-089-2959, which correspond to tetragonal anatase TiO₂ with structure parameters $a = b = 3.7822 \text{ \AA}$, $c = 9.5023 \text{ \AA}$, $\alpha = \beta = \gamma = 90.0^\circ$ and hexagonal titanium metal with crystal parameters $a = b = 2.9510 \text{ \AA}$, $c = 4.6820 \text{ \AA}$, $\alpha = \beta = 90.0^\circ$, $\gamma = 120.0^\circ$, respectively. Only Ti peaks appeared in amorphous TNTs at $2\theta = 38.40^\circ$, 40.17° , and 53.00° , which corresponds to (002), (101) and (102) planes. For 450 °C TiO₂, prominent peaks can be seen at $2\theta = 25.325^\circ$, 38.244° and 53.087° , which can be indexed correspondingly to diffraction from (101), (112) and (105) planes, respectively, and for major titanium the diffraction is observed at $2\theta = 40.091^\circ$ and 52.995° , which corresponds to the (101) and (102) planes, respectively. It is confirmed that the as-prepared TNTs are amorphous and 450 °C TNTs are

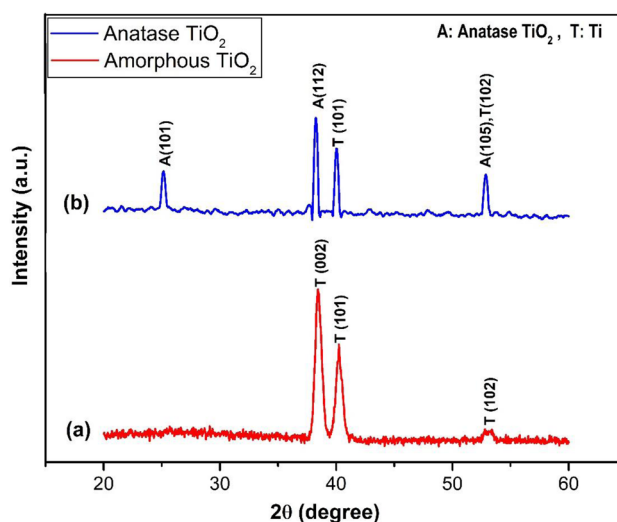


Fig. 1 XRD patterns of single-step **a** as-prepared amorphous TiO₂ nanotubes (TNTs), **b** annealed at 450 °C

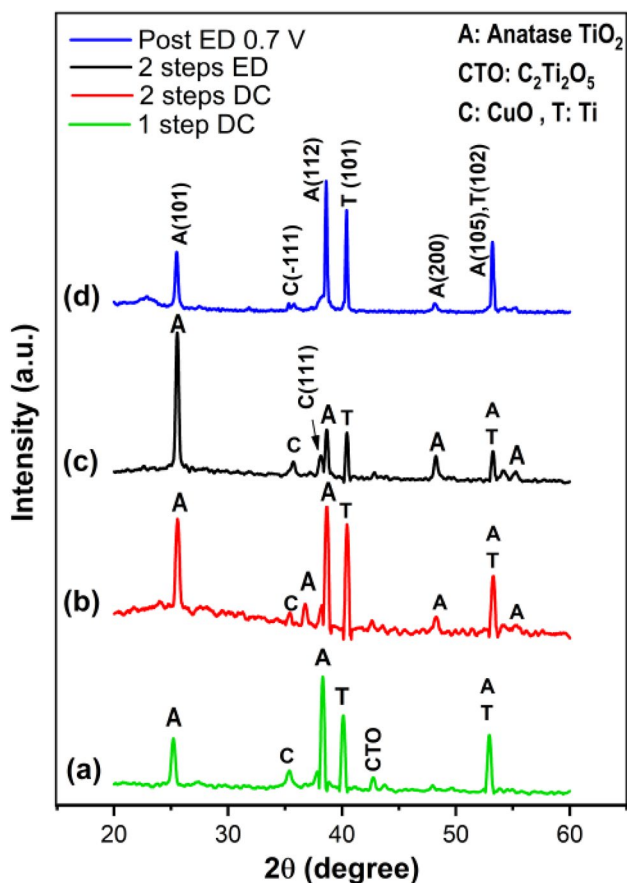


Fig. 2 XRD patterns of CuO-loaded ATNTs **a** synthesized by one-step anodization and modified by dip coating, **b** synthesized by two-step anodization and modified by dip coating and **c** synthesized by two-step anodization and modified by electrodeposition at 0.7 V. **d** The XRD pattern of 0.7 V electrodeposited sample after photoelectrochemical measurements

anatase phase crystalline TiO_2 , which are successfully grown on the titanium substrate.

Figure 2 demonstrates the CuO-loaded ATNTs. Figure 2a refers to JCPDS Card No. 01-084-1286 of the anatase phase TiO_2 , and the peaks at $2\theta = 25.584^\circ$, 38.690° , 48.262° and 53.247° correspond to reflection from the (101), (112), (200) and (105) planes, respectively. While from JCPDS Card No. 01-089-2959, the peak at $2\theta = 40.380^\circ$ and 53.01° corresponds to the reflection from the (101) and (102) planes of titanium substrate. Two additional peaks at $2\theta = 35.350^\circ$ and 38.213° are observed which are identical to the peaks of JCPDS Card No. 01-089-2531 of monoclinic copper oxide (CuO) with lattice parameters $a = 4.6691$ Å, $b = 3.4805$ Å, $c = 5.1183$ Å, $\alpha = \gamma = 90.0^\circ$, $\beta = 98.5980^\circ$. These two peaks confirm the successful loading of CuO on ATNTs. The peak at $2\theta = 42.72^\circ$ matches with JCPDS card no. 00-024-0340, which

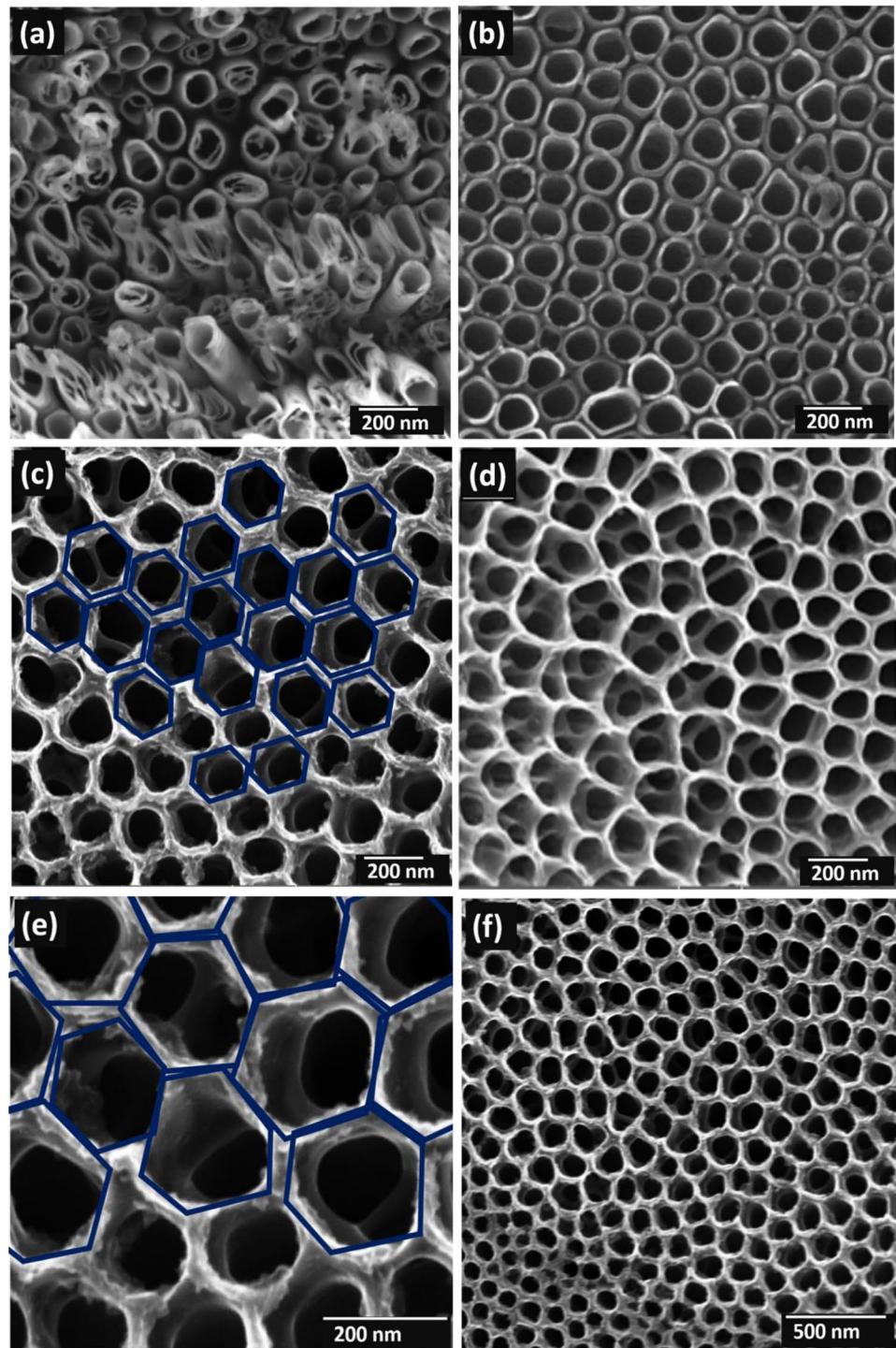
corresponds to the formation of copper titanium oxide ($\text{Cu}_2\text{Ti}_2\text{O}_5$) above 100°C according to the above JCPDS card no.

Figure 2b shows the XRD pattern of two-step anodized TNTs modified by dip coating. The peaks match with the same JCPDS of cards in Fig. 2a with additional two anatase peaks at $2\theta = 36.76^\circ$ and 55.17° , corresponding to the (103) and (211) planes, respectively. The peak at $2\theta = 53.89^\circ$ corresponds to $\text{Cu}_2\text{Ti}_2\text{O}_5$. Figure 2c shows the XRD diffractogram of 0.7 V electrodeposited CuO/TiO_2 TNTs. All the peaks are similar to that in Fig. 2b with almost the same peak positions. It is confirmed that CuO is successfully loaded in one- and two-step anodized anatase phase of TiO_2 by both dip coating and electrodeposition. It can be concluded that the junctions TiO_2 -CuO are successfully formed which was our objective for the photocatalytic hydrogen generation. To confirm that the TiO_2 -CuO heterojunctions are stable to photo corrosion, the XRD pattern of the 0.7 V electrodeposited sample was recorded after the photoelectrochemical (PEC) measurements and is shown in Fig. 2d. All the reflections from the anatase phase of TiO_2 and monoclinic CuO phase can be observed in the post-PEC sample, suggesting the aqueous and photocorrosion stability of the heterojunctions.

SEM analysis

FE-SEM analysis was performed for morphological examination of thin film of titania nanotubes (TNTs). In Fig. 3, the difference between the morphology of one- and two-step anodized TiO_2 nanotubes and their variation with annealing temperature are depicted. It can be observed that the nanotubes grown by both one- and two-step anodization are vertically oriented to the plane of the Ti substrate, well organized and compact. Moreover, the walls of the nanotubes grown by single-step anodization (shown in Fig. 3a and b.) are smooth, while the walls of two-step anodized nanotubes have a clear step blow at a certain depth from their surfaces as shown in Fig. 3c–f. The step in the walls of two-step TNTs may be due to additional growth on the imprints of one-step anodized TNTs. Also, the openings of one-step anodized nanotubes are nearly circular, but hexagonal (as fitted by blue color hexagons) for most of the two-step anodized TNTs. The effect of shifting from circular to hexagonal openings of TNTs has also been reported by other authors as well (Li et al. 2009; Macak et al. 2007; Zhang et al. 2007, 2010). Most of the amorphous one-step anodized TNTs have spiral shape circular openings, which modified into regular circular shapes when annealed at 450°C as depicted in Fig. 3a and b, respectively. The average diameter of the openings of one-step anodized TNTs are larger than 115 nm with average tube-wall thickness of ~ 20 nm.

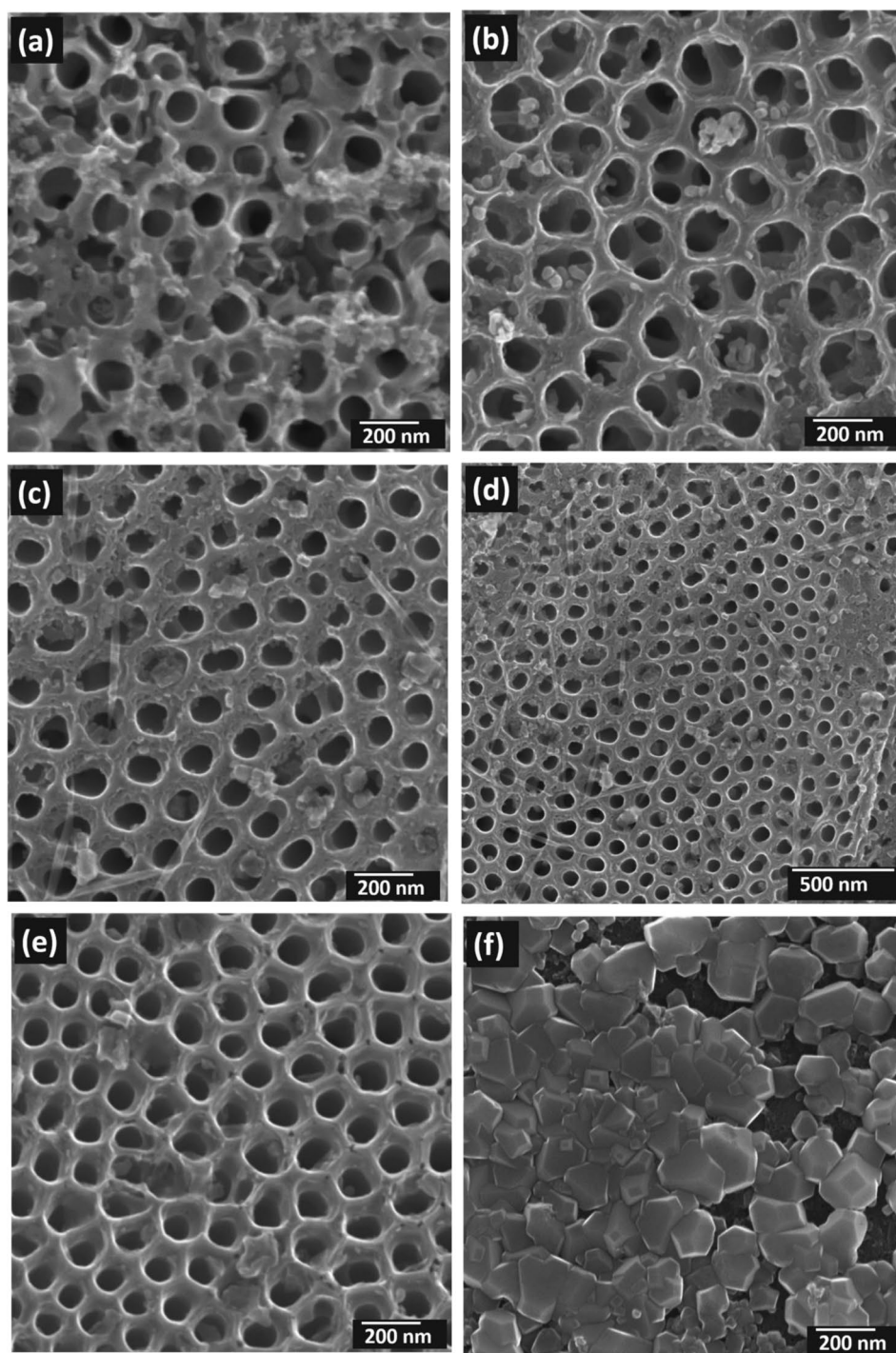
Fig. 3 SEM images of **a** one-step anodized amorphous TNTs at resolution of 150 kX, **b** one-step anodized anatase TNTs at resolution of 150 kX, **c** two-step anodized amorphous TNTs at resolution of 150 kX, **d** two-step anodized anatase TNTs at resolution of 300 kX and **e** two-step anodized anatase TNTs at resolution of 80 kX



The sizes of the openings of two-step anodized TNTs increased up to 170–200 nm. However, the wall thickness of two-step anodized TNTs of the nanotubes decreased from 10 to 13 nm. The void density also decreased in two-step TNTs, due to decrease in wall thickness and increase in the sizes of nanotube openings. The film of TNTs developed through single step is loosely attached to the titanium substrate and easily wears out by surface

bending or surface scratch. It may be associated to the spiral openings and water molecules present in the titania crystallites which evaporate after annealing. The thin film of two-step anodized TNTs become more robust and hard with annealing and have good adhering property to the titanium substrate, compared to one-step anodized TNTs. From nanotubes' morphology, it can be clearly predicted that two-step anodized titania nanotubes are promising

Fig. 4 SEM images of **a** one-step anodized dip-coated CuO/ATNTs, **b** two-step anodized dip-coated CuO/ATNTs, **c** two-step anodized 0.7 V electrodeposited CuO/ATNTs at 200 nm resolution, **d** two-step anodized 0.7 V electrodeposited CuO/ATNTs at 500 nm resolution, **e** two-step anodized 0.9 V electrodeposited CuO/ATNTs and **f** two-step anodized 1.1 V electrodeposited CuO/ATNTs



hosts for easy incorporation of other nanoparticle species, due to their large and regular opening sizes.

Figure 4 shows one- and two-step anodized TNTs modified by CuO nanoparticle by dip coating and electrodeposition methods. It can be observed in Fig. 4a that some of the CuO nanoparticles with average size less than 20 nm are successfully inserted into the nanotube openings and in the voids of one-step anodized ATNTs, while most of them are

accumulated on the tubes' surfaces. It can also be observed that the CuO nanoparticle loading is uneven on the surface of ATNTs with non-uniform penetration inside the tubes. The purpose of washing with DI after single dip was to remove the surface precursor, but still most of it can be seen on the surface with a higher density. In the two-step ATNTs, most of the CuO nanoparticles are properly inserted in the tubes as shown in Fig. 4b. The proper penetration of CuO

nanoparticles in two-step ATNTs is because of the relatively wider openings of the tubes. Due to unevenness in the walls of the ATNTs, most of the particles are observed to be stuck in the step seen in the walls of the ATNT arrays. However, it was observed that the CuO nanoparticles loosely connected with ATNTs and were not in intimate contact with them.

Figure 4c shows the two-step ATNTs, followed by CuO nanoparticles electrodeposited at 0.7 V applied potentials using Gamry potentiostat. A better coverage and contact of the CuO nanoparticles are seen over and inside ATNTs. During electrodeposition, the required energy for the reaction is provided by the voltage, which spreads uniformly over the entire ATNTs. The deposited CuO nanoparticles thus established atomic contacts with the ATNTs by electrostatic forces, which is a foremost requirement in making p–n junctions. The deposits also spread uniformly and have lesser chances of agglomeration, which results in relatively even incorporation of CuO nanoparticles. It can also be depicted that very fine particulates of sizes not greater than 10 nm are electrodeposited at this applied bias. The surface coverage of CuO nanoparticles is also greater than that observed for dip-coated samples as also seen in Fig. 4d (resolution of 80 kX and 500 nm).

At 0.9 V, the electrodeposition becomes non-uniform with relatively larger CuO nanoparticles as can be seen in Fig. 4e. The nanoparticle of CuO becomes highly agglomerated at 1.1 V applied potential and almost all of them just cover the surface of nanotubes and result in blockage of the openings of the nanotubes as shown in Fig. 4f. The reason for higher agglomeration at 0.9 V and 1.1 V may be due to the excessive energy supplied by biasing, which results in accumulation of CuO nanoparticles with themselves instead of with ATNTs. Therefore, it can be concluded that among the three applied potentials, 0.7 V is optimum for the required, suitable and uniform modification of CuO nanoparticles in ATNTs.

Energy-dispersive X-ray (EDX) spectroscopy

EDX analysis was performed to check the elemental composition of anodized ATNTs and the confirmation of CuO modification in it. Three abundant elements, i.e., Ti, O and Cu peaks, can be observed in the EDX spectrum of all the modified ATNTs as shown in Fig. 5. Nitrogen peaks may also be seen in Fig. 5b, c and d, which may be due to the presence of nitrogen supply during characterization.

The Cu peaks in all the ATNTs confirm the successful modification of CuO in all ATNTs as also confirmed by XRD and SEM. The Cu peak in two-step dip-coated CuO–ATNTs (Fig. 5b.) is larger than that in one-step anodized dip-coated CuO–ATNTs (Fig. 5a.) as also confirmed by FE-SEM images. This clearly indicates more CuO loading in two-step ATNTs than in one-step ATNTs by dip

coating. The 0.7 V electrodeposited two-step CuO–ATNTs as presented in Fig. 5c shows the EDX spectrum having Cu peak strength more or less the same as that of two-step dip-coated CuO–ATNTs (Fig. 5b). This shows that the amount of CuO loading is almost the same in both the CuO/ATNTs. In the 0.9 V electrodeposited two-step CuO–ATNTs (Fig. 5d), the Cu peak height is lower than that of 0.7 V electrodeposited two-step CuO–ATNTs, as also confirmed by the respective FE-SEM images in (Fig. 4e). Figure 6f shows the EDX spectra of 1.1 V electrodeposited two-step CuO–ATNTs, showing the highest of all Cu peaks than all other CuO–TNTs. It shows the high surface coverage of CuO on the surface of ATNTs, as also shown in their FE-SEM image (Fig. 4f).

Contact angle measurement

Contact angle measurement of titanium metal and ATNTs was performed to confirm their hydrophobic and hydrophilic nature, respectively. For contact angle measurement, a water drop was put on the surface of Ti and ATNTs. The measured average contact angles are 77.46 and 13.74 for Ti substrate and ATNTs, respectively, as shown in Fig. 6. These results confirm that the nature of ATNTs is hydrophilic and that of Ti substrate is near to hydrophobic. The Ti metal surface once oxidized develops polar dangling bonds on the surface which help to impart it wettability; therefore, the nature of Ti shifts from hydrophobic to hydrophilic after being oxidized. The hydrophilicity is a very important and essential property for ATNTs to be used as photoelectrode for water splitting. Due to hydrophilic nature, more water molecules will be in contact with the TiO₂ surface and more number of reaction sites will be produced.

Water splitting

For assessing the photocurrent responses of different samples of TiO₂ nanotubes, the photocurrent densities (PCDs) were measured versus applied voltage (vs Ag/AgCl) in the voltage range of 0.0–1.0 V both in dark and in light exposure from solar simulator with intensity 1000 W/m². From Fig. 7a, it can be observed that PCDs is negligible for all pristine TiO₂ nanotubes in the dark; therefore, all PCDs are represented by the same representative curve. The amorphous TNTs show lower PCDs responses than the anatase TNTs in the presence of light as shown in Fig. 7b and c. PCDs of amorphous two-step anodized TNTs is 1.25 times higher than the amorphous one-step anodized TNTs in the irradiance of light. Because of higher conductivity of the anatase phase of TiO₂, the PCDs of ATNTs are higher than that of amorphous TNTs as depicted in Fig. 7d and e. The conductivity of two-step anodized ATNTs is 1.20 times higher than that of one-step ATNTs. Because of the open

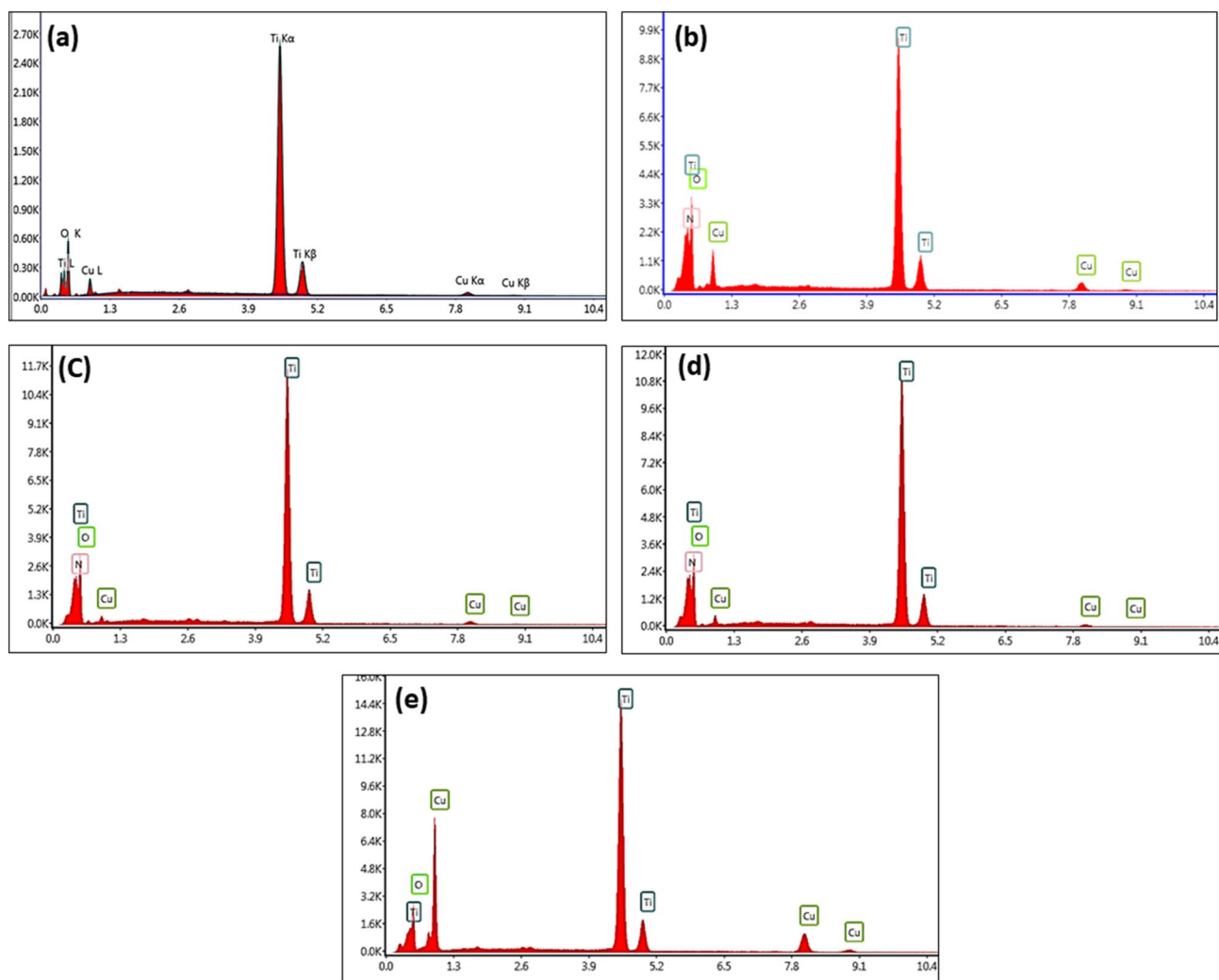


Fig. 5 EDX spectra of CuO-modified **a** one-step anodized ATNTs, two-step, **b** dip-coated ATNTs, **c** 0.7 V electrodeposited ATNTs, **d** 0.9 V electrodeposited ATNTs and **e** 1.1 V electrodeposited ATNTs

top nanotubes obtained by two-step anodization, the CuO/ATNTs heterojunction formation is easier that will result in more surface reaction sites and PCDs. The two-step anodized ATNTs have the highest applied bias to photocurrent

efficiency of 1.37% and hydrogen generation rate of $1.11 \mu\text{mol}/\text{cm}^2/\text{h}^1$.

The PCDs responses of CuO-loaded ATNTs versus applied voltages are represented in Fig. 8. The PCDs in dark is negligible similar to pristine TNTs/ATNTs. Dip-coated

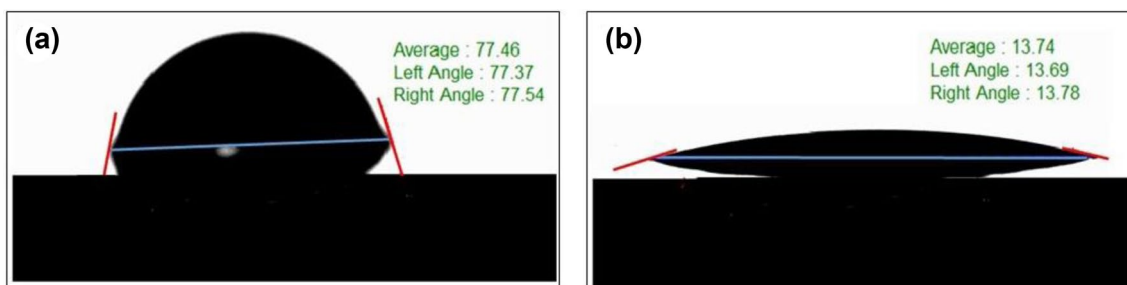


Fig. 6 Surface contact angle measurement of **a** titanium, **b** anodized titania nanotubes

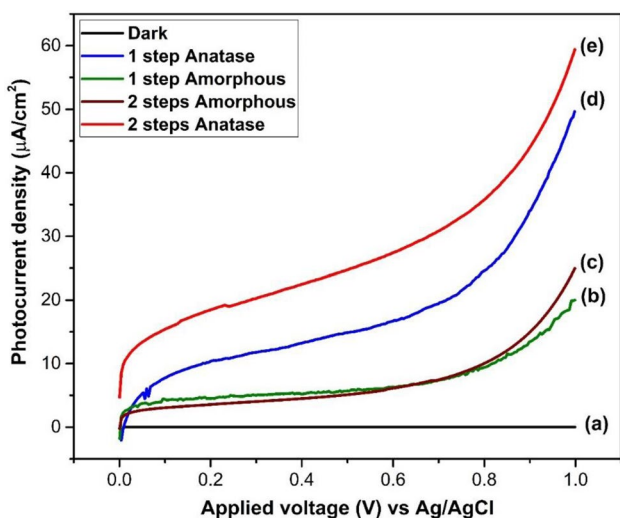


Fig. 7 Photocurrent densities of pristine TNTs **a** in dark for all samples, in the presence of solar simulator light, **b** one-step anodized amorphous, **c** two-step anodized amorphous, **d** one-step anodized anatase and **e** two-step anodized anatase TNTs

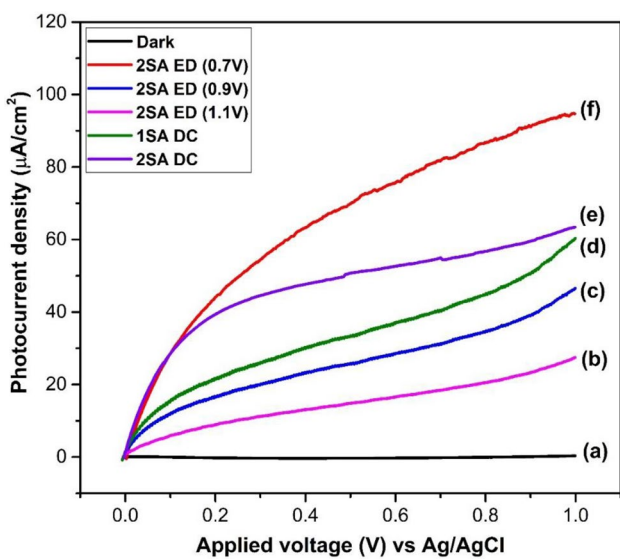


Fig. 8 Photocurrent densities of CuO-loaded **a** all ATNS samples in dark, in the presence of solar simulator light, **b** two-step anodized ATNTs loaded by electrodeposition at 1.1 V, **c** two-step anodized ATNTs loaded by electrodeposition at 0.9 V, **d** one-step anodized ATNTs loaded by dip coating, **e** two-step anodized ATNTs loaded by dip coating, **f** two-step anodized ATNTs loaded by electrodeposition at 0.7 V

two-step anodized ATNTs shows 1.06 times higher photocurrent density (PCD) as compared to dip-coated one-step ATNTs as depicted in Fig. 8d and e. This confirms the an easy and proper formation of p–n junction of p-type CuO and n-type TiO₂ in the case of two-step anodized ATNTs due to their broader openings than one-step anodized ATNTs.

The CuO-loaded ATNTs by electrodeposition show different PCDs at different electrodeposition voltages. The 0.7 V electrodeposited ATNTs show the highest PCD of 94.72 µA/cm² at 1.0 V vs Ag/AgCl, which is 2.02 and 3.42 times the PCDs of 0.9 V electrodeposited and 1.1 V electrodeposited ATNTs, respectively, as shown in (Fig. 8b,c). The lower PCDs of 0.9 V and 1.1 V electrodeposited samples may be due to excessive attractive force provided by biasing voltage which results in the agglomeration of nanoparticles with their self on the surface of nanotubes. This agglomeration obstructs the seeping of water into the tubes and results in lower PCDs.

The 0.7 V electrodeposited two-step CuO–ATNTs show 1.48 and 1.57 times higher PCD as compared to dip-coated two-step and one-step ATNTs, respectively, as shown in Fig. 8f, e and d. The photocurrent densities of electrodeposited CuO/TiO₂ TNTs are also separately plotted in Fig. 9. The higher PCD of 0.7 V electrodeposited CuO/TiO₂ TNTs may be due to the formation of proper p–n junctions by electrostatical attachment of CuO nanoparticles with the wall of nanotubes. The biasing applies a uniform electrostatic attractive force between the CuO nanoparticles and ATNTs, due to which they stick uniformly to the walls of the nanotubes. In contrast, by the dip-coating method, the CuO nanoparticles just reside on tubes and penetrate under gravity inside the nanotubes up to short distances. Therefore the p–n junctions of dip-coated CuO–TNTs/ATNTs are weak with respect to the junction produced by electrodeposition.

To confirm that the photocurrent responses of all the samples is solely due the photocatalytic water splitting, the on–off data were recorded for all pristine and CuO-modified samples. The light from the solar simulator was chopped by

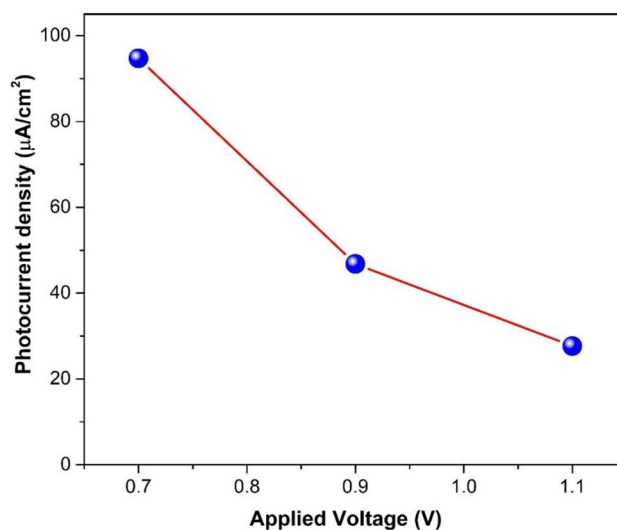


Fig. 9 Photocurrent densities of CuO-loaded two-step ATNT at 1.0 V vs Ag/AgCl

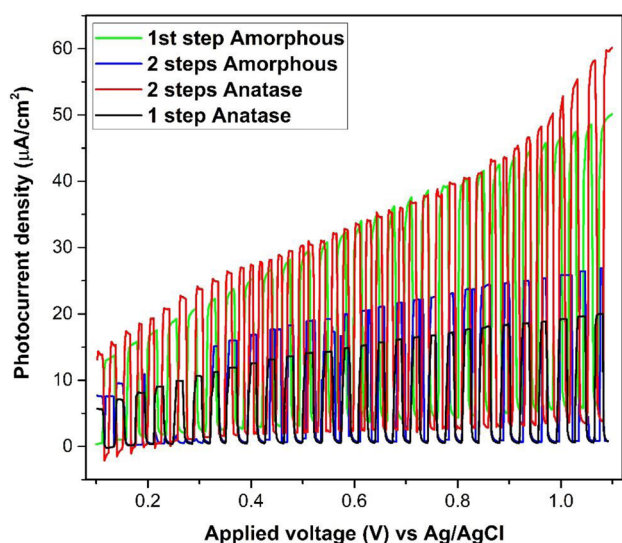


Fig. 10 On–off photocurrent densities of pristine TNTs/ATNTs

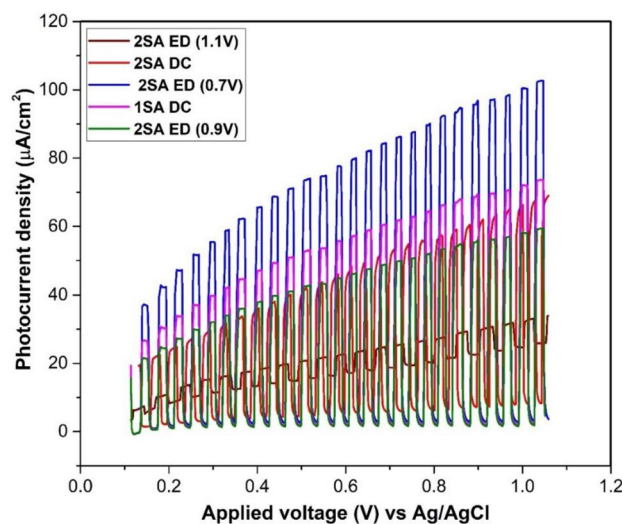


Fig. 11 On–off photocurrent densities of modified CuO/TiO₂ ATNTs

Table 1 Summary of the LSV results

Nature of sample	Sample name	Photocurrent density ($\frac{\mu\text{A}}{\text{cm}^2}$) at 0.1 V vs. Ag/AgCl	ABPE (%)	H ₂ ($\frac{\mu\text{mol}}{\text{cm}^2\text{h}^{-1}}$)
Pristine TNTs/ATNTs	Dark	0.003	6.9×10^{-5}	5.5×10^{-6}
	1st step amorphous	20.08	0.46	0.37
	2nd step amorphous	25.15	0.58	0.47
	1st step anatase	49.58	1.14	0.92
	2nd step anatase	59.46	1.37	1.11
	CuO-modified ATNTs	2SA ED 0.7	94.72	2.18
2SA ED 0.9		46.79	1.15	0.87
2SA ED 1.1		27.66	0.64	0.52
1SA DC		60.26	1.39	1.12
2SA DC		64.03	1.47	1.20

a handmade manual chopper at regular intervals in the range 0.1–1.1 V vs. Ag/AgCl.

When the light was chopped, photocurrent densities of all samples dropped to their corresponding dark current densities. Under illumination, the photocurrent densities rise to higher values as shown in Figs. 10 and 11. It confirms that the recorded photocurrent densities are mainly caused by photocatalytic water splitting, because the photocurrents for all the samples were measured in distilled water in the absence of any sacrificial agent.

The applied bias to photocurrent efficiency (ABPE) of the various photoanodes used was calculated using the equation:

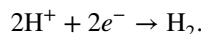
$$\text{ABPE} = \left(\frac{J_p \times (1.23\text{V} - |V_{\text{bias}}|)}{P_{\text{in}}} \times 100 \right) \%$$

where J_p refers to the photocurrent density (mA/cm^2), V_{bias} is the applied bias between the working electrode and counter electrode (V), and P_{in} is the incident illumination power density (AM 1.5 G, $100 \text{ mW}/\text{cm}^2$). The term 1.23 is used for the minimum theoretical potential or Gibbs free energy required for water splitting.

Using the heterogeneous electrode, the hydrogen production rate per unit area is calculated (Bard et al. 2000):

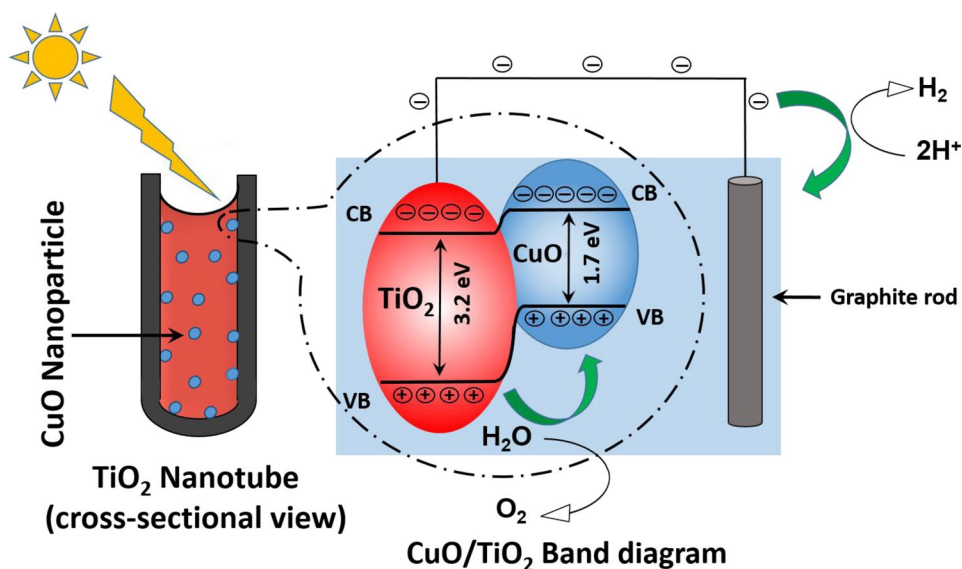
$$H (\text{mol hr}^{-1} \text{cm}^{-2}) = \frac{J_p}{nF} \times 3600,$$

where H is the hydrogen production rate, J_p is the photocurrent density (A/cm^2), F is the Faraday constant ($96,485.33 \text{ C}/\text{mol}$) and n is the number of number of electrons involved in the production of a single hydrogen molecule, that is,



As evident from the above chemical reaction that one mole of hydrogen requires two moles of electrons, therefore, $n = 2$. All of these results are listed in Table 1.

Fig. 12 Schematic of the band diagram CuO–TiO₂ p–n junction



Mechanism of photocurrent density enhancement with CuO modification

Anatase TiO₂ has a large band gap of 3.2 eV which requires a light source with wavelength less than 387.45 nm to excite an electron from valence band to conduction band. Therefore, suitable band gap engineering is necessary to utilize visible light for excitation. CuO, being a small band gap (1.7 eV) p-type semiconductor, on making a junction with an n-type TiO₂, reduces the band gap resultantly. Consequently, the photocurrent enhances and causes more water splitting. The overall mechanism is shown in Fig. 12.

Conclusion

TiO₂ nanotubes (TNTs) are synthesized by one- and two-step anodization of the Ti substrate. Dip-coating and electro-deposition (at 0.7 V, 0.9 V and 1.1 V) methods are used for CuO nanoparticles modification in anodized anatase phase titania nanotubes (ATNTs). Structural characterizations (FE-SEM, EDX and XRD) confirmed the successful synthesis of TiO₂ nanotubes and their modification with CuO nanoparticles. SEM revealed the circular and hexagonal openings of one- and two-step anodized TNTs/ATNTs. Contact angle measurement confirmed the hydrophilic nature of TNTs/ATNTs, which is necessary for water splitting applications. Photocatalytic water splitting results show that photocurrent responses of all TNTs/ATNTs are low in both pristine and modified form. Photocurrent densities of anatase phase TNTs are 2.46 and 2.36 times higher than that of amorphous one- and two-step anodized TNTs, respectively. Because of the wider openings, the photocurrent density of two-step anodized ATNTs is 1.20 times higher than that of one-step ATNTs. The two-step anodized ATNTs have the highest

applied bias to photocurrent efficiency of 1.37% and hydrogen generation rate of 1.11 μmol/cm²/h¹, which is higher than that of all other pristine TNTs. Dip-coated two-step anodized ATNTs show 1.06 times higher photocurrent density as compared to dip-coated one-step ATNTs. There is better performance of two-step anodized ATNTs than one-step anodized ATNTs when dip coated by CuO. The 0.7 V electrodeposited ATNTs show the highest photocurrent density of 94.72 μA/cm² at 1.0 V vs Ag/AgCl, which is 2.02 and 3.42 times the photocurrent densities of 0.9 V and 1.1 V electrodeposited ATNTs, respectively. The 0.7 V electrodeposited two-step CuO–ATNTs show 1.48 and 1.57 times higher PCD as compared to dip-coated two-step and one-step ATNTs, respectively. It can be concluded that two-step anodized anatase phase TiO₂ nanotubes (ATNTs) are better to be used in pristine and CuO-modified form than one-step anodized ATNTs. The method of electrodeposition at optimum 0.7 V has been proved to be superior for CuO nanoparticles loading in ATNTs than the dip-coating method.

Acknowledgements The authors are grateful to the Higher Education Commission of Pakistan (20-3684/R&D/HEC/14) and Pakistan Science Foundation (PSF/NSFC-Eng/KP-COMSATS-ABT-04) for financial support.

Compliance with ethical standards

Conflict of interest The authors declare no conflict of interest.

References

Bard AJ, Faulkner LR, Leddy J (2000) Electrochemical methods: fundamentals and applications, 2nd edn. Wiley, New York

- Ge M, Cao C, Huang J, Li S, Chen Z, Zhang KQ, Al-Deyab SS, Lai Y (2016) A review of one-dimensional TiO₂ nanostructured materials for environmental and energy applications. *J Mater Chem A* 4(18):6772–6801. <https://doi.org/10.1039/c5ta09323f>
- Hagiwara H, Nagatomo M, Ida S, Ishihara T (2012) Photocatalytic splitting of water into hydrogen and oxygen on organic dye modified KTa(Zr)O₃ catalyst. *Energy Procedia* 22:53–60. <https://doi.org/10.1016/j.egypro.2012.05.224>
- Hashimoto K, Irie H, Fujishima A (2005) TiO₂ photocatalysis: a historical overview and future prospects. *Jpn J Appl Phys Part 1 Regul Pap Short Notes Rev Pap* 44(12):8269–8285. <https://doi.org/10.1143/JJAP.44.8269>
- Kudo A, Miseki Y (2009) Heterogeneous photocatalyst materials for water splitting. *Chem Soc Rev* 38(1):253–278. <https://doi.org/10.1039/b800489g>
- Li S, Zhang G, Guo D, Yu L, Zhang W (2009) Anodization fabrication of highly ordered TiO₂ nanotubes. *J Phys Chem C* 113(29):12759–12765. <https://doi.org/10.1021/jp903037f>
- Lin HY, Chang YS (2010) Photocatalytic water splitting for hydrogen production on Au/KTiNbO₅. *Int J Hydrogen Energy* 35(16):8463–8471. <https://doi.org/10.1016/j.ijhydene.2010.06.006>
- Liu Y, Zhou B, Bai J, Li J, Zhang J, Zheng Q, Zhu X, Cai W (2009) Efficient photochemical water splitting and organic pollutant degradation by highly ordered TiO₂ nanopore arrays. *Appl Catal B* 89(1–2):142–148. <https://doi.org/10.1016/j.apcatb.2008.11.034>
- Macak JM, Albu SP, Schmuki P (2007) Towards ideal hexagonal self-ordering of TiO₂ nanotubes. *Phys Status Solidi RRL Rap Res Lett* 1(5):181–183. <https://doi.org/10.1002/pssr.200701148>
- Nguyen TH, Nguyen TL, Ung TDT, Nguyen QL (2013) Synthesis and characterization of nano-CuO and CuO/TiO₂ photocatalysts. *Adv Nat Sci Nanosci Nanotechnol* 4(2):1–6. <https://doi.org/10.1088/2043-6262/4/2/025002>
- Ni M, Leung MKH, Sumathy K, Leung DYC (2006) Potential of renewable hydrogen production for energy supply in Hong Kong. *Int J Hydrogen Energy* 31(10):1401–1412. <https://doi.org/10.1016/j.ijhydene.2005.11.005>
- Paramasivam I, Nah Y-C, Das C, Shrestha NK, Schmuki P (2010) WO₃/TiO₂ nanotubes with strongly enhanced photocatalytic activity. *Chem Eur J* 16(30):8993–8997. <https://doi.org/10.1002/chem.201000397>
- Praveen Kumar D, Shankar MV, Mamatha Kumari M, Sadanandam G, Srinivas B, Durgakumari V (2013) Nano-size effects on CuO/TiO₂ catalysts for highly efficient H₂ production under solar light irradiation. *Chem Commun* 49(82):9443–9445. <https://doi.org/10.1039/c3cc44742a>
- Puangpetch T, Sommakettarin P, Chavadej S, Sreethawong T (2010) Hydrogen production from water splitting over Eosin Y-sensitized mesoporous-assembled perovskite titanate nanocrystal photocatalysts under visible light irradiation. *Int J Hydrogen Energy* 35(22):12428–12442. <https://doi.org/10.1016/j.ijhydene.2010.08.138>
- Rasheed MA, Rahimullah R, Uddin SK, Khaliq N, Khan Y, Waheed A, Shah A, Mahmood A, Ali G (2019) Role of temperature and NiO addition in improving photocatalytic properties of TiO₂ nanotubes. *Appl Nanosci (Switzerland)* 9(8):1731–1742. <https://doi.org/10.1007/s13204-019-00980-z>
- Razali MH, Yusoff M (2018) Highly efficient CuO loaded TiO₂ nanotube photocatalyst for CO₂ photoconversion. *Mater Lett* 221:168–171. <https://doi.org/10.1016/j.matlet.2018.03.100>
- Seong DB, Son YR, Park SJ (2018) A study of reduced graphene oxide/leaf-shaped TiO₂ nanofibers for enhanced photocatalytic performance via electrospinning. *J Solid State Chem* 266:196–204. <https://doi.org/10.1016/j.jssc.2018.06.003>
- Wold A (1993) Photocatalytic properties of titanium dioxide (TiO₂). *Chem Mater* 5(3):280–283. <https://doi.org/10.1021/cm00027a008>
- Xie MY, Su KY, Peng XY, Wu RJ, Chavali M, Chang WC (2017) Hydrogen production by photocatalytic water-splitting on Pt-doped TiO₂-ZnO under visible light. *J Taiwan Inst Chem Eng* 70:161–167. <https://doi.org/10.1016/j.jtice.2016.10.034>
- Zhang G, Huang H, Zhang Y, Chan HLW, Zhou L (2007) Highly ordered nanoporous TiO₂ and its photocatalytic properties. *Electrochem Commun* 9(12):2854–2858. <https://doi.org/10.1016/j.elecom.2007.10.014>
- Zhang Z, Hossain MF, Takahashi T (2010) Photoelectrochemical water splitting on highly smooth and ordered TiO₂ nanotube arrays for hydrogen generation. *Int J Hydrogen Energy* 35(16):8528–8535. <https://doi.org/10.1016/J.IJHYDENE.2010.03.032>
- Zhang J, Li L, Zhang J, Zhang X, Zhang W (2017) Controllable design of natural gully-like TiO₂-ZrO₂ composites and their photocatalytic degradation and hydrogen production by water splitting. *New J Chem* 41(17):9113–9122. <https://doi.org/10.1039/c7nj00511c>

Publisher's Note Springer Nature remains neutral with regard to jurisdictional claims in published maps and institutional affiliations.